DEVELOPMENTAL BIOLOGY **192,** 630–644 (1997)
ARTICLE NO. DB978741

Germ-Layer Surface Tensions and "Tissue Affinities" in *Rana pipiens* Gastrulae:

Grayson S. Davis,* Herbert M. Phillips,† and Malcolm S. Steinberg‡,[1]

**Department of Biology, Valparaiso University, Valparaiso, Indiana 46383; †Fertility Institute of Boca Raton, Boca Raton, Florida 33428; and ‡Department of Molecular Biology, Princeton University, Princeton, New Jersey 08544*

The morphogenetic properties causing germ-layer spreading and stratification in amphibian gastrulation were called "tissue affinities" by Holtfreter. The differential adhesion hypothesis (DAH) attributes such liquidlike tissue rearrangements to forces generated by intercellular adhesions within and between the migrating cell populations. This theory predicts that, among the primary germ layers, the cohesiveness of deep ectoderm should be the greatest, that of deep mesoderm should be intermediate, and that of deep endoderm should be the least. Also, the cohesiveness of differentiating neural ectoderm should increase after induction, causing it to internalize and segregate from epidermis. The DAH also explains why the cohesiveness of "liquid" tissues, whose cells are free to rearrange, should be measurable as tissue surface tensions. Using a specially designed tissue surface tensiometer, we demonstrate that (i) aggregates of *Rana pipiens* deep germ layers do possess liquid-like surface tensions, (ii) their surface tension values lie in precisely the sequence necessary to account for germ-layer stratification *in vitro* and *in vivo,* and (iii) the surface tension of deep ectoderm just underlain by the archenteron roof is twice that of not-yet-underlain deep ectoderm. These measurements provide direct, quantitative evidence that the "tissue affinities" governing germ-layer flow during early stages of vertebrate morphogenesis are reflected in tissue surface tensions.

> "If we arrange the embryonic tissues according to their degree of cohesion we have to put the ectoderm and its derivatives, the epidermis and the neural plate, at the top of the list, the endoderm at the bottom, and the mesoderm in between."
> p. 198 in Holtfreter (1944)

INTRODUCTION

Like all rearrangements of matter, the tissue redistributions during vertebrate gastrulation and neurulation must have a mechanical basis. Lying originally side-by-side, the prospective germ-layer regions move *en masse* until ectoderm completely covers endoderm, with mesoderm and neural tissue sandwiched in-between. What forces direct and propel these embryonic tissue migrations?

Holtfreter's pioneering experiments (Holtfreter, 1939) demonstrated that recombined explants from amphibian embryos engage in autonomous, combination-specific rearrangements which mimic *in vivo* gastrulation, exogastrulation, neurulation, and early organogenesis. To distinguish the class of *short range* interactions governing these movements from other types of morphogenetic mechanisms (e.g., differential growth), Holtfreter proposed for them the term "tissue affinities" ("Gewebeaffinität"; Holtfreter, 1939). These phenomena occurred "while the various kinds of cells and tissues were in direct mutual contact" and acted "as a means of self-ordering of embryonic regions," accounting for "local migration and constriction movements in whole cell complexes, starting with those in gastrulation and being continued through organogenesis." Later, Townes and Holtfreter (1955) reported that even randomly reaggregated mixtures of dissociated cells can spontaneously rearrange to assume normal germ-layer stratification.

Holtfreter proposed several possible mechanistic bases for "tissue affinities," including differences in cell adhesiveness and "directed movement"—"a kind of cytotactic reaction of the proximal cell surfaces to a gradient of interfacial

[1] To whom correspondence should be addressed. Fax: (609) 258-1547. E-mail: msteinberg@princeton.edu.

0012-1606/97 $25.00

tension between inside and outside of the embryo'' (Townes and Holtfreter, 1955). However, he did not conduct experiments designed to distinguish among these. Ultimately he favored a chemotactic model (reviewed in Steinberg, 1996). However, details of the behavior of aggregates of isolated and recombined embryonic tissues strongly supported a different mechanism: (i) When irregularly shaped pieces of many embryonic tissues are cultured on nonadhesive substrata, they gradually round up into spherical shapes. (ii) When two such aggregates from different amphibian or chick embryonic tissues are placed in mutual contact, they usually fuse, one spreading around the other in a tissue-specific envelopment pattern (reviewed in Steinberg, 1964; Armstrong, 1989). (iii) When cells from those same tissues are dissociated and reaggregated, they sort out from one another, approaching the same final configuration attained after fusion of the undissociated tissue masses (Townes and Holtfreter, 1955; Steinberg, 1962c, 1963, 1970). (iv) This cell sorting proceeds by a specific pathway: the coalescence of smaller clusters of the internalizing component to form progressively larger clusters (Steinberg, 1962b; Trinkaus and Lentz, 1964; Glazier *et al.*, 1995; see also Townes and Holtfreter, 1955, Figs. 16 and 17). (v) Tissues' mutual envelopment tendencies are not unique to each combination but obey the rule of transitivity: they form an ''inside–outside'' hierarchy (Steinberg, 1962c, 1963, 1964, 1970; reviewed in Steinberg, 1964, and in Armstrong, 1989; see also Heintzelman *et al.*, 1978).

Steinberg (1962a,b,c, 1963, 1964, 1970) demonstrated that these phenomena do not conform with expectations based upon a chemotactic model, but instead closely resemble the rounding-up, droplet spreading, and phase separation behavior seen in systems of immiscible, viscous liquids. Such behavior in ordinary liquids is controlled by specific interfacial free energies (surface and interfacial tensions) arising from the intensities of intermolecular attractions (e.g., Adamson, 1967). The ''differential adhesion hypothesis'' (DAH) proposes (i) that liquid-like tissue spreading and cell sorting are controlled by corresponding *tissue* surface tensions[2] (Steinberg, 1962c, 1963, 1964, 1970; Phillips, 1969; Foty *et al.*, 1994, 1996) and (ii) that those movements and physical properties arise from type-specific differences in the intensities of adhesions between motile cells which repeatedly exchange weaker for stronger adhesions (Steinberg, 1962a,b,c; Phillips, 1969, 1984; Steinberg and Takeichi, 1994). That the stated cell properties suffice in theory to generate the observed tissue spreading and cell sorting behavior has been elegantly and realistically demonstrated by computer simulations (Glazier and Graner, 1993; Mombach *et al.*, 1995). Tissue surface tension measurements, in various multicellular systems, not only provide a critical experimental test of this physical explanation for the guidance of liquid–tissue flow, but may also help to identify the responsible adhesive molecules. The present experiments were carried out to determine whether amphibian germ layers possess liquid-like surface tensions whose relative values correspond with those predicted by the DAH (Steinberg, 1962c, 1964, 1970; Phillips, 1969, 1984; Phillips and Davis, 1978; Davis, 1984) to produce their observed mutual spreading and the resulting stratification of the early embryo.

Since a liquid of lower surface tension will tend to spread around an immiscible liquid of higher surface tension, any tissue which tends to envelop another tissue is predicted to have the lower surface tension of the two (Steinberg, 1962c; Phillips, 1969). Surface tension, a liquid's resistance to increases in its surface area, can be measured by deforming a liquid droplet and then monitoring its final, equilibrium shape as a function of the applied force (Adamson, 1967). By definition, surface tensions of liquids must be *area-invariant*. Therefore, during successive deformations of a liquid interface, measured surface tension values must remain constant for each increment of applied force and resulting surface area expansion. This differs from the response of elastic solid materials, which display incrementally increasing resistance to surface area expansion when they are deformed (Adamson, 1967).

Applying the above analysis to amphibian germ-layer stratification requires an understanding of Holtfreter's distinction between ''coated'' and subsurface cells. Holtfreter (1943, 1944) demonstrated that the apical surfaces of the cells of the amphibian blastula, some of which involute to form the lining of the archenteron, are nonadhesive to other cells. He called this region, recognizable at present as the contiguous apical domains of this epithelial sheet, the ''surface coat'' and demonstrated that cells bearing it are forced, by its nonadhesiveness, to lie at free surfaces. Thus, unlike the immediately subjacent region of the same germ layer, a ''coated'' cell layer cannot be enveloped by any other tissue. Fragments of the deeper (''uncoated'') tissues combined *in vitro* display tissue-specific spreading behavior in which ectoderm segregates internally to mesoderm, which segregates internally to endoderm (Holtfreter, 1944; Townes and Holtfreter, 1955; Phillips and Davis, 1978). This is the opposite of normal germ-layer architecture. When ''coated'' ectoderm is present in explants, as it is in the embryo, this pattern is reversed so that typical germ-layer stratification ensues (Holtfreter, 1944; reviewed in Phillips and Davis, 1978).

Our present study utilizes only samples of *subsurface* germ-layer tissues. Application of the DAH to these cell populations yields the following three experimentally testable predictions: (i) Isolates of deep (''uncoated'') gastrula ectoderm, mesoderm, and endoderm should have classically defined (area-invariant) surface tensions. (ii) Their surface tension values should fall into the sequence: deep ectoderm $>$ deep mesoderm $>$ deep endoderm, reflecting the mutual spreading tendencies of these ''uncoated'' tissues. (iii) Since neural ectoderm is enveloped by neighboring tissues after

[2] Throughout this paper, ''tissue surface tension'' will be used in an inclusive sense to refer to tensions both at tissue–medium and tissue–tissue interfaces.

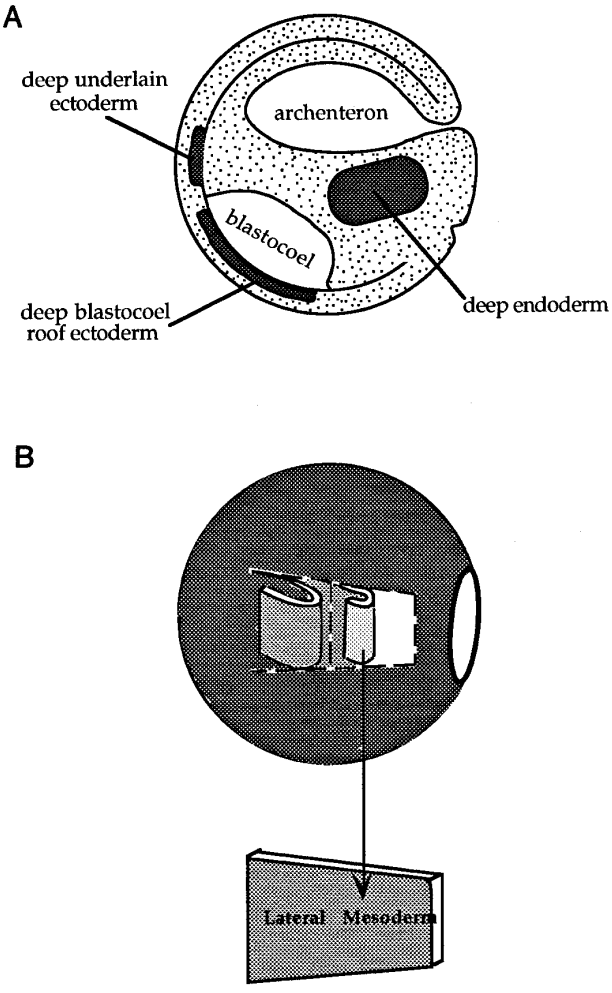

FIG. 1. Diagrams of a stage 11+ embryo illustrating locations of the cell populations used in this study. (A) Median sagittal section showing locations of deep blastocoel roof ectoderm, adjacent deep ectoderm underlain by the advancing roof of the archenteron, and deep subarchenteric endoderm. (B) Surface view (left side) showing location of deep lateral mesoderm (dissected).

its induction by the advancing archenteron roof, the surface tension of induced deep, presumptive neural ectoderm should become greater than that of adjacent (uninduced) deep ectoderm. The experiments reported here were designed to test these predictions.

MATERIALS AND METHODS

Animals, Embryos, and Tissues

Rana pipiens (J. M. Hazen Co., Alburg, VT, and Charles D. Sullivan Co., Nashville, TN) were kept at 4°C in 25% amphibian Ringer's solution (Rugh, 1962) containing 200 μg/ml neomycin sulfate (0.86 ml/liter Biosol; Upjohn Co., Kalamazoo, MI). Egg laying was induced by intraperitoneal injection with one or two fresh or two to 18 lyophilized frog pituitaries (Carolina Biological Supply Co., Burlington, NC); then eggs were artificially fertilized (Rugh, 1962).

Mid-yolk-plug embryos (Shumway [1940] stage 11+) were dejellied with forceps (Hamburger, 1960) in 10% modified Steinberg's solution (SS, Poole and Steinberg, 1977) and were transferred to dissecting dishes coated with 1–8% oxoid-purified agar (Unipath Ltd., Basingstoke, England), and filled with full-strength SS, pH 7.4. Vitelline membranes were then removed gently with sharpened watchmakers' forceps (Jacobson, 1967).

In each dissection, the "coated" surface cells were first peeled with tungsten needles and hairloops from the region of interest and discarded. The underlying deep tissue was then excised with hairloops and cut into pieces of the desired size, which were then cultured in fresh medium (SS) at 21°C until they rounded up.

Ectoderm, mesoderm, and endoderm were operationally defined by position, relative cell size, and pigmentation. Ectoderm cells were small and darkly pigmented, mesoderm cells were larger and less pigmented, and endoderm cells were very large and unpigmented. Border regions of ambiguous cell size and color were not used. Locations of cell populations used in this study (Fig. 1) coincide with the positions of subsurface anterior ectoderm, lateral involuted mesoderm, and subarchenteric endoderm mapped by Vogt (1929) for *Rana esculenta* and *Rana fusca.*

Parallel-Plate Compression Measurements of Tissue Surface Tensions

Rounded-up aggregates of subsurface ectoderm, mesoderm, and endoderm were compressed in SS, one at a time, between parallel plates in a chamber that permits measurement of the applied force of compression. The lower plate was a 2-mm square chip of glass coverslip epoxy-cemented to the end of a flexible quartz fiber (Polymicro Technologies Inc., Phoenix, AZ) approximately 100 μm in diameter and 6 cm in length. Both this quartz fiber and a more rigid tungsten rod (Aldrich Chemical Co., Milwaukee, WI), approximately 250 μm in diameter and 7 cm in length, were glued at one end into the tip of a glass tube partly filled with epoxy cement. The free, electrolytically sharpened tip of the rod was bent toward the chip. This appliance constituted a fiber-rod assembly (FRA; Fig. 2).

When an FRA was oriented as in Fig. 2, any vertical force applied to the top of the chip bent the fiber away from its resting position and moved the chip closer to the tip of the rod. Since the rod remained immobile, the deflection of the quartz fiber was equal to the change in the rod–chip distance, illustrated in Fig. 2. The bending constant (K) was determined empirically for each rod by placing preweighed pieces of aluminum foil on the chip and measuring

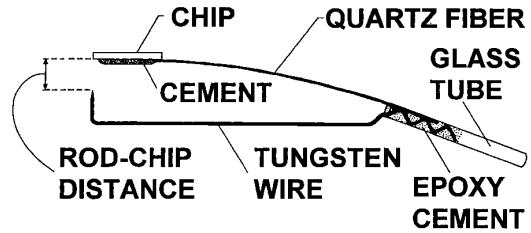

FIG. 2. A fiber-rod assembly.

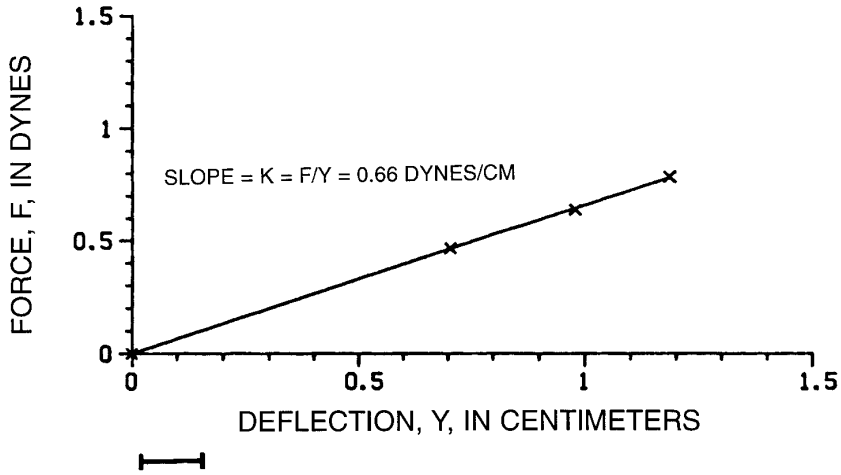

FIG. 3. Graph of force applied (by loading the chip with various standard weights) versus deflection of chip from its unloaded position, for a typical fiber-rod assembly. (Bracket illustrates range of deflections needed to compress the aggregates used in this study.)

rod–chip distances with a traveling microscope. The deflection (Y) of the chip was always observed to be directly proportional to the force (F) applied,

$$F = KY, \qquad [1]$$

where K is the constant of proportionality (Hooke's constant) (Fig. 3). This linear relationship indicates that these quartz fibers obeyed Hooke's law precisely throughout and well beyond the range of deflections used in our experiments.

Several FRAs were firmly clamped onto movable holders suspended from the roof of the aggregate-compression chamber (Fig. 4) which we designed and constructed for use in this study. Height and angle adjustments of the FRAs were provided by means of separate controls on each holder. These controls were initially set so that the chip was oriented horizontally approximately 1 cm below the surface of the culture medium (SS) at 21°C. After the assemblies and their holders were clamped into the chamber, a glass plate was lowered into the medium just above the chip. Both the chip and plate had been previously coated with 1% oxoid agar which had been allowed to cool and solidify before immersion in the medium. A stereomicroscope and a front-surfaced mirror placed at a 45° angle in the chamber provided an end-view of the chip, the plate, and the pointed tip of the rod. The stereomicroscope was adjusted with respect to the mirror until a precisely vertical image of the chip and rod was obtained. Alternatively, a compound microscope focused through the glass plate provided a top view of the aggregate and chip.

After rounding up for 3 to 12 h in culture, a spherical aggregate was gently pipetted onto the chip and the initial distance between the chip and the tip of the rod was recorded through the stereomicroscope. The aggregate was then gently compressed by raising the FRA holder until the aggregate contacted the agar-coated glass plate and was perceptibly deformed. A timed series of profile photographs or camera lucida tracings of the rod–chip distance and of the vertical profile of the aggregate was then made through the stereomicroscope. For ectoderm and mesoderm, three successive determinations were generally made on each aggregate with forces sufficient to compress the aggregate first to roughly seven-eighths of its original height, then to approximately three-fourths, and finally to approximately one-half of its original height. In some cases, a third compression became impossible if the chamber was jostled, an air bubble formed on the FRA (changing its buoyant density) or an aggregate began to adhere to and actively spread upon an improperly

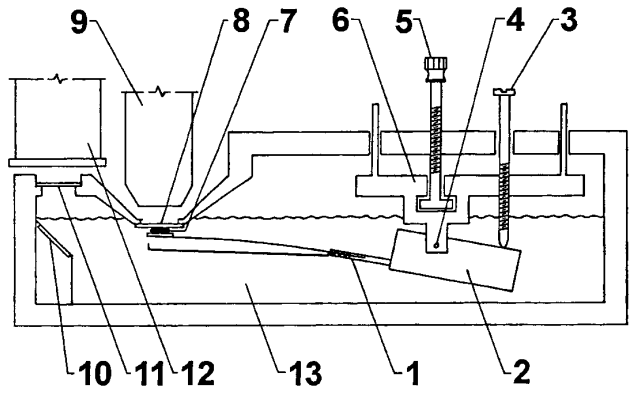

FIG. 4. Parallel-plate compression chamber. The fiber-rod assembly (1) is clamped into a holder (2). Turning the angle-adjusting control (3) raises or lowers the rear end of the holder. This rotates the holder about its pivot (4), tilting the assembly so that the chip can be leveled. Turning the height-adjusting control (5) raises the movable platform (6). This elevates the holder, causing the chip to press the aggregate (7) against the glass plate (8). The objective of a compound microscope (9) (not used in final S measurements) provides top views of the aggregate through the glass plate. Alternatively, a 45°-angle front-surfaced mirror (10) reflects a side-view image of the aggregate and an end-view image of the rod and chip through the viewing port (11) to a stereomicroscope (12). The aggregate and the fiber-rod assembly are completely immersed in culture medium (13).

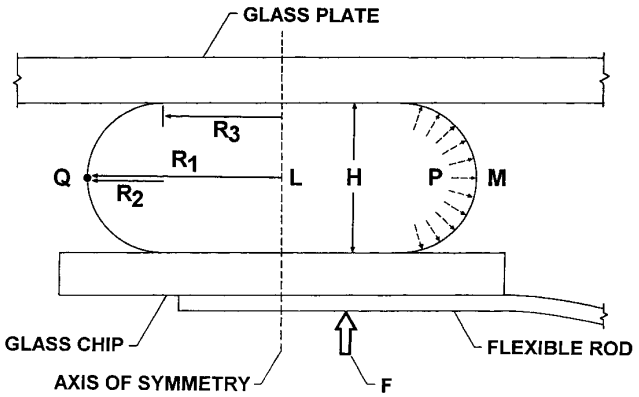

FIG. 5. A liquid specimen (L) in medium (M) is compressed between two parallel plates to which it does not adhere. P is the pressure difference across the L–M interface, and σ in Eq. [3] is the surface tension of that interface. R_3 is the radius of the area of contact of either plate with L. R_1 is the radius of horizontal curvature and R_2 is the radius of vertical curvature at point Q on the "equator." The height (H) of the specimen equals the distance between the parallel plates. The force of compression (F) can be determined from the deflection of the flexible rod (see Materials and Methods).

coated region of the compressing surface. In the case of endoderm aggregates, only two determinations could be made because of that tissue's fragility. After the last determination, the holder was lowered until the aggregate separated from the upper plate. Another photograph was then taken of the final position of the rod and chip. The data were utilized only if the rod–chip distance was the same before and after aggregate compression.

Measurements of aggregate shape parameters and the distance between the rod and chip were calculated from tracings of photographs or camera lucida drawings taken with the stereomicroscope through the viewing port. For determinations of the force and shape equilibrium (see Fig. 8), the radii of vertical curvature (R_2 in Fig. 5) on the left and right sides of the aggregate profile were assessed by comparisons with a series of circular arcs of known radii drawn on transparent plastic. The radii of successive standard arcs differed by 2%. For each side of an aggregate, R_2 was calculated as the average of the radii of the larger and smaller standard arcs which best matched that side of the aggregate tracing. For the calculation of surface tension values, camera lucida drawings or tracings of photographs of aggregates were digitized by means of a Summagraphics Summasketch pad (for which a software driver was generously provided by Dr. J. Sorenson of Butler University) connected to a personal computer. The coordinate values of the traced lines were analyzed by an adaptation of a program generously provided by Dr. R. Gordon of the University of Manitoba. Right-side and left-side values of R_2 were averaged for each aggregate to obtain a mean value of its vertical radius of curvature.

To determine the accuracy of our procedures, similar force–shape measurements were made on compressed air bubbles. The chamber was filled with air-saturated distilled water and an air bubble was pipetted onto the lower surface of the plate. A small bubble was used so that the bubble was not noticeably deformed by the buoyancy holding it against the plate before compression. Each bubble was compressed to several different heights, providing measurements of applied force and resultant shape as described above for the cell aggregate compressions.

Scanning Electron Microscopy

For scanning electron microscopy (SEM), a smaller and simpler chamber, employing a single, inflexible FRA, was used to fix aggregates during compression between parallel, agar-coated surfaces. After 1, 5, or 15 min of compression, aggregates were fixed by gently adding 4% formaldehyde in SS in a volume equal to that of the culture medium already in the chamber. After 15 min of fixation, compressed aggregates were removed from the device and fixation was continued for another 2 h. Uncompressed pieces of tissue were fixed by pipetting them into a large volume of 2% formaldehyde fixative in SS. All aggregates were washed overnight in SS plus 3.5% sucrose, dehydrated with ethanol, which was replaced with amyl acetate, and then were critical point dried in liquid CO_2. All were attached to stubs with silver conducting paint and coated with approximately 100 Å of gold before examination at 15 kV. Tracings of vertical profiles of compressed aggregates from SEMs were measured as above for determinations of equilibrium. The heights of compressed aggregates were also measured from those micrographs.

RESULTS

Test of the Tissue Surface Tensiometer and Methods of Measurement

Small air bubbles (1.0 to 1.5 mm in diameter) in air-saturated distilled water did not spread appreciably on the agar-coated surface of the glass plate in the compression chamber (Fig. 6A). Since the bubbles were larger than our cell aggregates, smaller portions of their profiles were obscured by the compressing surfaces. In fact, if the compressing surfaces were positioned at a slight angle so that, instead of being parallel to each other, they opened toward the mirror, almost all of a bubble's vertical radius could be photographed before the bubble "squirted" out from between the compressing plates. Bubbles photographed in this way appeared to have semicircular vertical curvatures (Fig. 6B). The chip and plate were then positioned parallel to each other so that the bubbles could be serially compressed to obtain plots of force versus shape. Because shape equilibrium was reached immediately, only one time point (1–3 min) after each compression was used for measurements of rod–chip distance and bubble shape. The mean of the reciprocals of the slopes for 17 compressions of two bubbles was 70.6 dyne/cm, which is within 3% of the published value of 72.75 dyne/cm for the surface tension of the air–water interface (Hodgman, 1958).

Rounding Up of Cell Aggregates

In hundreds of cases, when irregularly shaped pieces of deep ectoderm, mesoderm, and endoderm were cultured on agar, they rounded up into nearly spherical shapes (Fig. 7), a behavior that is characteristic of liquid droplets. Ectoderm

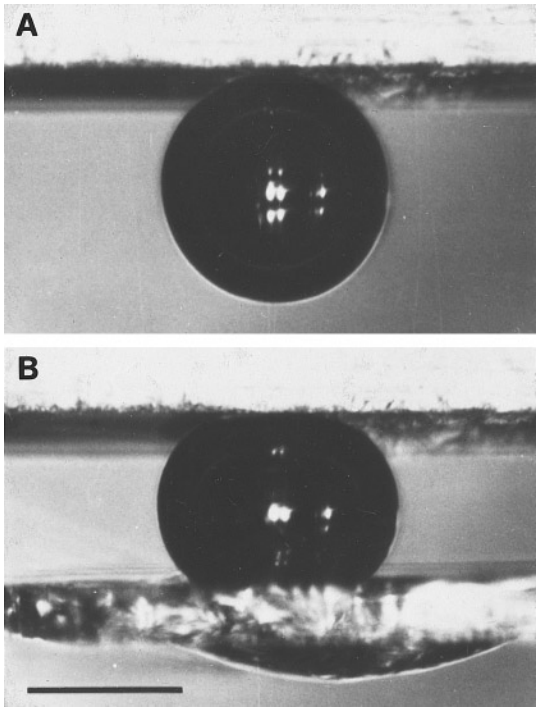

FIG. 6. (A) An air bubble held by its own buoyancy against the glass plate in the compression chamber. (B) A similar bubble during slight compression, with the compressing surfaces angled toward the mirror, providing maximum visibility of the bubble's profile. Bar represents 0.5 mm.

and mesoderm explants required approximately 3 h to round up; endoderm explants required approximately 4 h.

Achievement of Force and Shape Equilibrium by Compressed Cell Aggregates

A parallel-plate compression chamber (Fig. 4) was used to study the time course of shape changes which such tissue masses undergo during compression. Figure 5 illustrates the theoretical shape of a liquid droplet compressed between parallel plates in such a chamber. In our experiments, initially spheroidal aggregates of gastrula deep ectoderm, mesoderm, and endoderm were compressed between agar-coated plates in such an assembly (see Materials and Methods). Measurements of applied force and resulting height indicated that changes in these parameters cease within 5 min of compression (more than 50 cases). However, since previous experiments (Phillips and Davis, 1978) had shown that complete relaxation of cell stretching in the interior of such compressed aggregates requires between 5 and 15 min, we began side-view monitoring of changes in force and in several parameters of aggregate shape at ten min of compression. Side-view photographs of aggregates were continued through 30 min (six cases) or 2 hr (two cases) of compression. No net changes in force (Fig. 8), radius of horizontal curvature, or radius of vertical curvature were observed after 10 min of compression. Therefore, shape equilibrium was achieved within 10 min of compression.

Characteristics of the Equilibrium Shape

Accurate measurements of R_3, the radius of the contact area, could not be made from side views of living, compressed aggregates. The out-of-focus images of the compressing surfaces, which extended beyond the depth of field of the microscope, blurred and partially obscured the contact region (Fig. 9). Also, the gap between the aggregate and the compressing surfaces becomes extremely narrow close to the region of contact. Its perimeter is therefore difficult to determine from either side or top views (Fig. 4), even under the best of circumstances (Yoneda, 1964; Adamson, 1967).

In principle, a liquid droplet compressed between two parallel plates to which it does not adhere should meet each plate at a contact angle of 180° (Adamson, 1967). Moreover, the vertical arc defining the side boundary of such a droplet should approximate a semicircle, so that the radius of the contact area of a compressed cell aggregate at shape equilibrium, R_3, could simply be calculated from R_1 and R_2 (see Fig. 5) as follows:

$$R_3 = R_1 - R_2. \qquad [2]$$

To evaluate the accuracy of this approximation, we examined the shapes of aggregates fixed during compression. It was first necessary to assess the effect of fixation on aggregate size and shape. In the fixation chamber, aggregates were compressed for 20 min—well after R_1 and R_2 stopped changing—and the aggregate profiles were photographed through the stereomicroscope just before fixation. After 15 min of fixation, the chips were lifted and the aggregates were removed, repositioned with their axes of symmetry perpendicular to the optical axis of the microscope, and then rephotographed without the compressing surfaces. Aggregates of deep ectoderm, mesoderm, and endoderm showed no detectable change in size or shape as a result of fixation (two cases for each tissue); aggregate profiles before and after fixation were congruent (Fig. 10A). These photographs gave the impression that the vertical curvatures of the aggregates did indeed approximate semicircles. If so, an arc of a circle with diameter equal to the height (H) of such a flattened aggregate should be superimposable upon the curved edge of the aggregate. Two such superimpositions, shown in Fig. 10B, demonstrate that the profiles of both sides of the fixed aggregate are almost perfect semicircles.

The tilting mechanical stage and superior resolution of the SEM permitted more precise observations of aggregate shape. Twenty compressed aggregates at shape equilibrium were fixed and SEMs showing their vertical profiles were prepared. The height (H) and vertical radius (R_2) of each side of every aggregate were measured directly (the latter

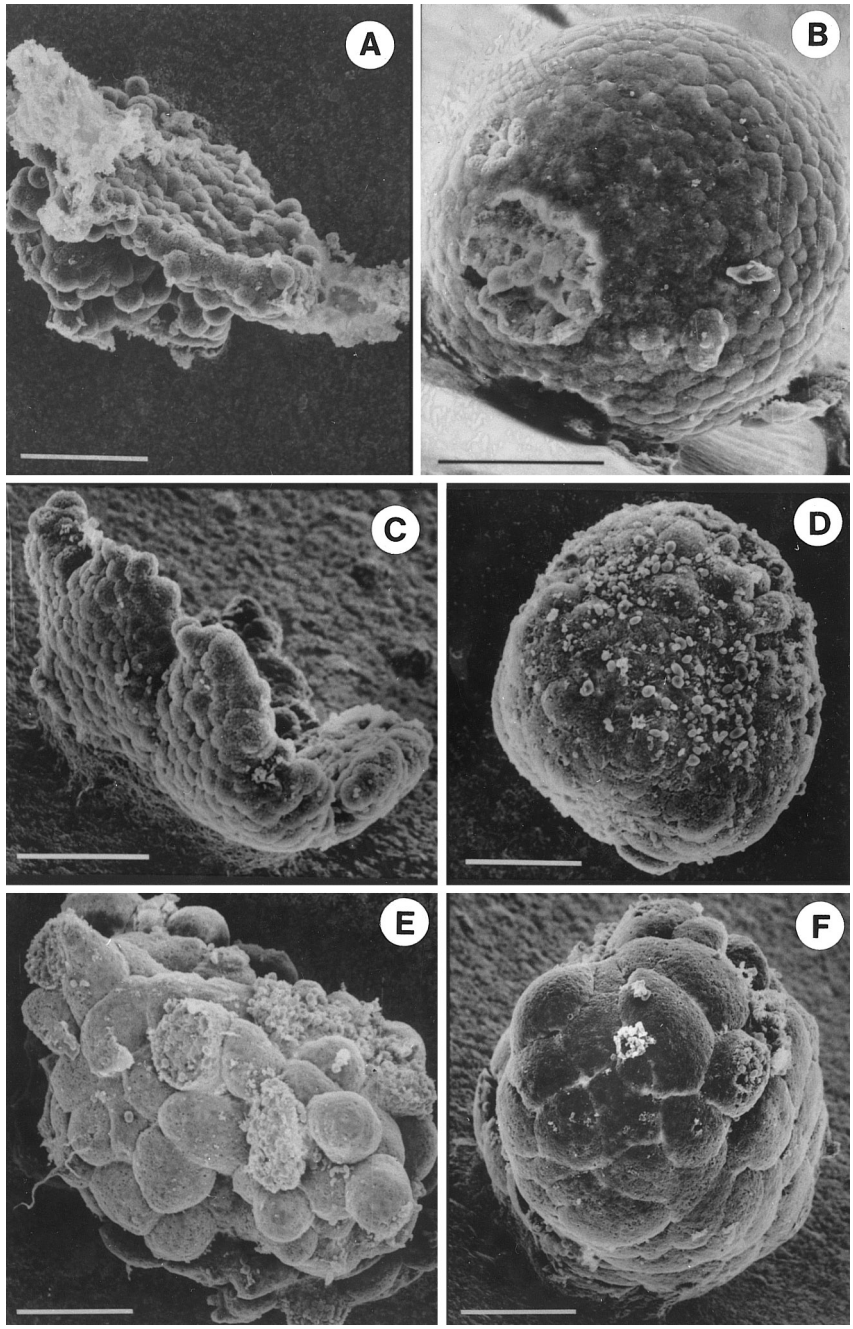

FIG. 7. SEMs of excised pieces of ectoderm (A, B), mesoderm (C, D), and endoderm (E, F). Tissues were fixed immediately after excision (A, C, E) or after 3 h (B, D) or 4 h (F) of culture on a nonadhesive agar substratum. Bars represent 0.1 mm.

by matching against a series of standard arcs) from tracings of these profiles. If the vertical curvature is not only an arc of a circle but also forms a complete half circle before intersecting the flattened top and bottom surfaces of the compressed aggregate, then the height of the aggregate should be equal to twice its vertical radius, so $2R_2/H$ should equal unity. Mean values of $2R_2/H$ for aggregates of all three germ layers are shown in Table 1. The significance of the difference between these values and unity was examined by Student's t test where, for the purposes of our analysis, P must be less than 0.05 to indicate statistical significance. The results ($P \geq 0.2$) demonstrate that the vertical curva-

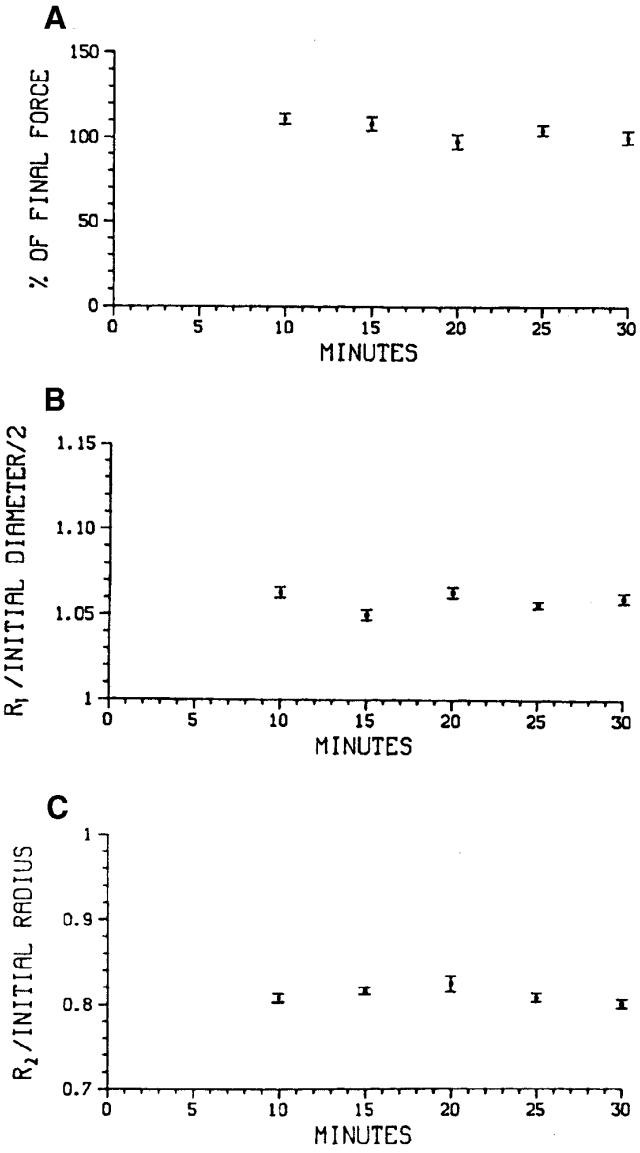

FIG. 8. The initial, precompression diameters (and therefore initial radii) of six spheroidal aggregates were determined from side-view photographs taken before parallel-plate compression. Additional photographs of the aggregates and corresponding rod–chip distances taken at various times during compression permitted sequential measurements of values of the force of compression (F), radius of horizontal curvature (R_1), and average radius of vertical curvature (R_2). The latter two parameters were obtained by manual curve-matching against a series of standard arcs. In graph A, the percentage of the final force (at 30 min) is plotted against time (duration of compression); in B, R_1/initial diameter/2 is plotted against time; in C, R_2/initial radius is plotted against time. The significance of the correlation (Pearson's r) between these variables and time reveals no significant change after 10 min (for percentage of final force versus time, $P = 0.17$; for R_1/initial diameter/2 versus time, $P = 0.48$; for R_2/initial radius versus time, $P > 0.90$). Bars indicate standard errors.

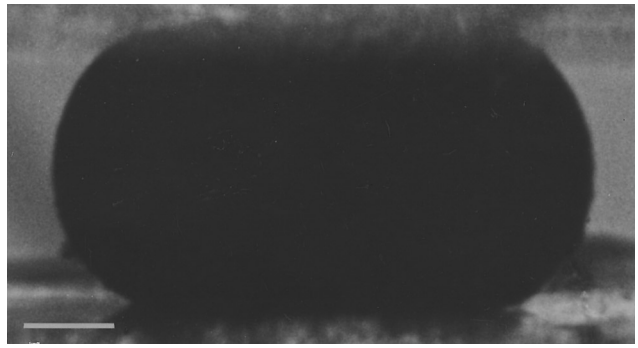

FIG. 9. Side view of a living mesoderm aggregate during parallel-plate compression. Bar represents 0.1 mm.

tures of these aggregates do not differ significantly from semicircles. Therefore, Eq. [2] can be applied to these aggregates with reasonable accuracy, allowing substitution of $R_1 - R_2$ for R_3—see Eq. [7] below.

Force versus Shape–Size

Compression of a liquid droplet between parallel plates to which it does not adhere offers a means for measuring surface tensions. Such a droplet has two principal radii of curvature, R_1 and R_2 (see Fig. 5). The force (F) applied by either of the parallel plates to deform the droplet is distributed over the contact area with the liquid (πR_3^2), balanced by the droplet's internal pressure, a function of its surface tension (σ) and its mean radius of curvature $[(1/R_1) + (1/R_2)]$. At shape equilibrium, these parameters are related by the equation,

$$\sigma = [F/(\pi R_3^2)]\,[(1/R_1) + (1/R_2)]^{-1}, \qquad [3]$$

derived from the Young–Laplace equation (Cole, 1932; Davis, 1984; Rowlinson and Widom, 1989; Foty *et al.*, 1994, 1996). Equation [3] can be written as

$$F = \sigma[(1/R_1) + (1/R_2)]\,(\pi R_3^2). \qquad [4]$$

We define S, a function of the size and shape of the aggregate, as

$$S = [(1/R_1) + (1/R_2)]\,(\pi R_3^2). \qquad [5]$$

Then, according to Eq. [4],

$$S = (1/\sigma)F. \text{ [see footnote 3]} \qquad [6]$$

[3] In the method of least squares, it is assumed that the independent variable can be determined more precisely than the dependent variable. Since measurements of F are more precise than measurements of S, it would have been inconvenient to write Eq. [6] as $F = \sigma S$.

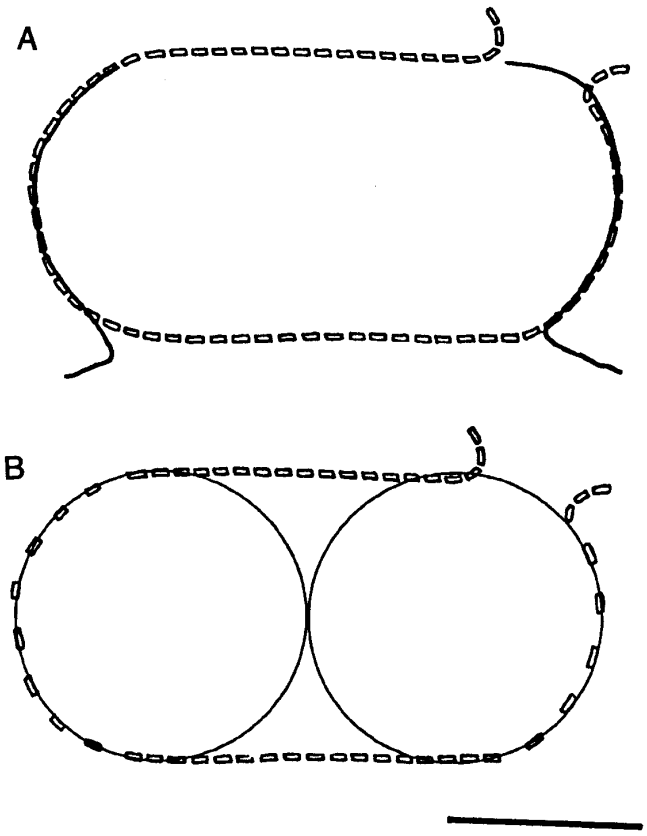

FIG. 10. (A) Profiles traced from two photographs of a single mesoderm aggregate. The solid line shows the shape of the living aggregate during compression in the fixation chamber. The dotted line shows the shape of the same aggregate after it has been fixed for 15 min and then removed from the compressing surfaces. Bar represents 0.1 mm. (B) Arcs of circles with diameter equal to the height of the flattened and fixed aggregate are shown superimposed upon profiles of its right and left sides (see Table 1).

Area Invariance of Aggregate Surface Tensions

Equations [3]–[6] require that surface tension (σ) be area-invariant, as it must be for any liquid (see Introduction). Therefore, σ should remain a constant of proportionality

TABLE 1

Comparison of R_2 with H, from SEM Profiles of Aggregates Fixed during Compression

Compressed aggregate	Number of cases	$2R_2/H \pm$ SE	$P(2R_2/H = 1)$
Deep ectoderm	12	1.04 ± 0.03	$P > 0.1$
Deep lateral mesoderm	4	1.03 ± 0.003	$P > 0.5$
Deep endoderm	4	0.99 ± 0.04	$P > 0.5$

Note. For a liquid droplet at shape equilibrium, $2R_2/H = 1$.

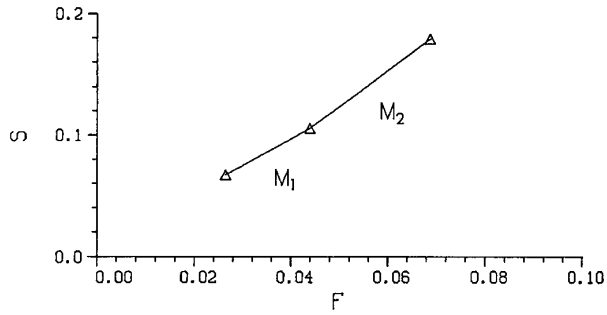

FIG. 11. Measured values at mechanical equilibrium of shape factor, S (in cm), plotted against force, F (in dynes), for a single mesoderm aggregate. The three points correspond to the three different degrees of compression: perceptibly different from spherical, approximately 3/4 of original height and approximately 1/2 of original height. M_1 is the slope of the line connecting the first two points, M_2 is the slope of the line connecting the second and third points.

for all paired equilibrium values of F and S, even as an aggregate's surface area varies with the extent of its compression. Hence, if a liquid specimen is compressed to different extents and then allowed to come to shape equilibrium, plots of S versus F should produce a straight line with constant slope equal to the reciprocal of the surface tension of that specimen. Rigorous testing of this relationship requires several compressions of a given aggregate. This could not be done for deep endoderm because it was too fragile to survive more than two compressions. Deep ectoderm and deep mesoderm aggregates were usually subjected to three successive compressions in the parallel-plate compression chamber. F, R_1, and R_2 were measured 15 min after the beginning of each compression. Values of F were obtained from Eq. [1]. Values of S were obtained from measurements of R_1 and R_2 using the combination of Eqs. [5] and [2]:

$$S = [(1/R_1) + (1/R_2)]\pi(R_1 - R_2)^2 \qquad [7]$$

A plot of S versus F for one aggregate is shown in Fig. 11. If the relationship between F and S is linear, then, for those aggregates subjected to three compressions, the slope (M_1) between the first two points should equal the slope (M_2) between the second and third points. Hence, the reciprocal of the slope, or surface tension (σ_1), between the first two points should equal the reciprocal of the slope (σ_2) between the second and third points. We therefore compared σ_1 with σ_2 for all aggregates with three compressions. For each of the three tissues examined in this way, we were unable to detect any statistically significant differences between σ_1 (average) and σ_2 (average); ($P_{\text{underlain ect}} > 0.17$; $P_{\text{lateral mes}} > 0.36$; $P_{\text{BCR ect}} > 0.76$). This confirms the first of the three predictions presented in the Introduction.

Values of Germ-Layer Surface Tensions

New measurements reported here were made upon rounded-up aggregates of deep ectoderm from two locations:

from the blastocoel roof and from the region lying immediately posterior to it in the median dorsal plane, underlain by the advancing archenteron. In addition, the earlier data for deep endoderm and deep lateral mesoderm (Davis, 1984), originally evaluated by manual curve matching, were reanalyzed by computer to improve reliability as described under Materials and Methods. Table 2 shows the surface tension of each tissue mass, calculated as the change in force divided by the change in *S*, for either the first and second compressions (first slope), the second and third compressions (second slope), or for all three compressions as the reciprocal of the slope of the regression (least squares fit) of *S* upon force (both slopes). Mean is the mean of the both slopes values for each tissue. For explants unable to survive a third compression, asterisks are entered and the first slope value alone is used as a both slopes value.

The mean surface tension values and standard errors for these tissues, reported in Table 2, are 0.36 ± 0.03 dyne/cm for deep endoderm, 0.56 ± 0.06 dyne/cm for deep lateral mesoderm, 0.80 ± 0.07 dyne/cm for deep blastocoel roof ectoderm, and 1.60 ± 0.25 dyne/cm for the deep ectoderm underlain by the archenteric roof immediately posterior to the blastocoel roof ectoderm. According to Student's *t* test, the probability that any of the observed differences in the mean values of these germ layer surface tensions is due to chance alone is less than 0.015. These results confirm the second and third of the three predictions presented in the Introduction.

The aggregates used in these experiments varied somewhat in size. The average precompression diameters and standard errors of a sample of four endoderm, four mesoderm, and eight blastocoel roof ectoderm aggregates were 0.47 ± 0.02, 0.44 ± 0.02, and 0.46 ± 0.03 mm, respectively. Although mean aggregate diameters were similar for each tissue, individual aggregate diameters differed by as much as 0.2 mm within a given tissue. To determine whether aggregate surface tensions were influenced by aggregate diameters, the latter were plotted against the former (not shown). As would be expected for liquid droplets, correlation coefficients from these plots failed to reveal a significant relationship between surface tension and size for any tissue ($r < +0.35$; $P > 0.50$ for each correlation, where $P < 0.05$ would be necessary to demonstrate correlation).

TABLE 2

Measured Surface Tension Values of Subsurface Germ Layer Samples

First slope	Second slope	Both slopes	Mean + SE
Endo[a]			0.36 ± 0.03 dyne/cm
0.26	—	0.26	
0.32	—	0.32	
0.34	—	0.34	
0.35	—	0.35	
0.44	—	0.44	
0.48	—	0.48	
⟨0.36⟩		⟨0.36⟩	
$Meso_{lateral}$			0.56 ± 0.06 dyne/cm
0.27	0.40	0.34	
0.50	0.24	0.35	
0.44	0.49	0.46	
0.70	0.43	0.52	
0.55	—	0.55	
0.69	0.50	0.57	
0.61	0.71	0.64	
0.69	0.64	0.66	
1.11	0.79	0.93	
⟨0.62⟩	⟨0.52⟩	⟨0.56⟩	
$Ecto_{BCR}$			0.80 ± 0.07 dyne/cm
0.29	0.17	0.25	
0.31	0.52	0.42	
1.26	0.29	0.49	
0.53	0.52	0.53	
0.45	0.69	0.56	
0.91	0.35	0.58	
0.59	—	0.59	
1.38	0.54	0.66	
0.69	—	0.69	
0.40	1.13	0.72	
1.17	0.60	0.72	
0.78	—	0.78	
0.83	—	0.83	
0.59	1.09	0.89	
3.06	0.59	0.92	
0.34	2.28	1.11	
1.78	0.90	1.14	
0.63	2.24	1.23	
1.29	—	1.29	
1.59	—	1.59	
⟨0.94⟩	⟨0.85⟩	⟨0.80⟩	
$Ecto_{underlain}$			1.60 ± 0.25 dyne/cm
1.50	0.55	0.79	
1.86	0.44	0.83	
0.72	2.58	0.92	
1.46	0.83	1.06	
2.95	0.73	1.33	
1.42	—	1.42	
1.61	1.55	1.57	
2.11	1.50	1.65	
3.04	1.44	1.92	
7.02	1.67	2.53	
3.08	4.45	3.57	
⟨2.43⟩	⟨1.57⟩	⟨1.60⟩	

[a] Reanalyzed from 1984 data.

DISCUSSION

Measurement of Tissue Surface Tensions

If rearrangements and final configurations of liquid-like embryonic cell populations are governed by adhesion-generated surface tensions as the DAH proposes (see Introduction), then tissues which segregate internally because of their greater cohesiveness should possess measurably higher surface tensions than do externally segregating (less cohesive) ones. Original efforts to test this hypothesis by direct physical measurements (Phillips, 1969; Phillips and

Steinberg, 1969) utilized prolonged, constant-speed centrifugation to press aggregates of embryonic chick cells against a nonadhesive substratum under organ-culture conditions. Like liquid droplets at rest in gravitational fields (sessile drops), centrifuged aggregates with higher surface tensions should resist deformation more (and so remain rounder) than do cell aggregates with lower surface tensions.

As predicted, initially flat aggregates were observed to round up against the centrifugal force and initially round aggregates were observed to flatten, both adopting the same final (equilibrium) shapes. Comparisons of the resulting equilibrium shapes of embryonic chick heart, limb bud, and liver provided the first experimental evidence of the postulated tissue-specific differences in the mechanical deformability of those multicellular aggregates (Phillips, 1969; Phillips and Steinberg, 1969). At identical centrifugal speeds, those tissues which became surrounded during aggregate spreading and cell sorting (Steinberg, 1962c, 1963, 1970)—''more cohesive'' tissues—did indeed adopt rounder shapes than did the surrounding, ''less cohesive'' tissues, precisely as deduced from the DAH (Phillips, 1969; Phillips and Steinberg, 1969). Also, when a given tissue's envelopment tendency was increased or decreased through experimental manipulations (Wiseman *et al.*, 1972), its centrifugal deformability changed correspondingly (Phillips *et al.*, 1977b).

In early aggregate-centrifugation experiments, the formation of a density gradient in the culture medium during prolonged centrifugation created uncertainties in the calculation of absolute values of tissue surface tensions (Phillips, 1969). A more convenient technique was subsequently devised: compression, by measured forces, of cell aggregates between parallel plates (Phillips and Davis, 1978). With that procedure, absolute surface tension values have recently confirmed and extended the sequence of relative tissue surface tensions reported by Phillips (1969) and Phillips and Steinberg (1969). Those absolute values range from 1.6 to 20.1 dyne/cm and continue to correlate exactly with the mutual envelopment behavior of the five embryonic chick cell populations examined (Foty *et al.*, 1994, 1996; Foty and Steinberg, 1995a,b).

The first application of the parallel plate compression procedure for the measurement of tissue surface tensions was made in a previous investigation of *R. pipiens* midgastrula tissues (Phillips and Davis, 1978). Under the same force of compression, deep mesoderm aggregates flattened more than deep ectoderm but less than deep endoderm, in agreement with the known mutual envelopment behavior of paired fragments of those tissues. Absolute values of tissue-medium surface tensions were later reported (in erg/cm^2, which is the equivalent of dyne/cm) as 2.92 ± 0.82 for deep ectoderm, 0.64 ± 0.09 for deep mesoderm, and 0.39 ± 0.03 for deep endoderm (Davis, 1984).[4] These values were calculated from the Young–Laplace equation by hand-matching photographic images of the compressed aggregates' vertical and horizontal profiles against circles of known radii. Those same images of deep mesoderm and deep endoderm have here been digitized and computer-analyzed to obtain the revised values of aggregate-medium surface tensions for deep mesoderm (0.56 ± 0.06 dyne/cm) and deep endoderm (0.36 ± 0.03 dyne/cm) presented in Table 2. As discussed below, the data given for ectoderm, both from the blastocoel roof and underlain by the archenteric roof, are new.

The high standard error (28%) of the earlier surface tension value for ectoderm (Davis, 1984) prompted a reexamination of that tissue, various samples of which had been taken from a rather broad region overlying the roof of the blastocoel anteriorly and the advancing roof of the archenteron posteriorly. We suspected that those fragments of ectoderm which had been in contact with the leading edge of the archenteron wall might have undergone a change in surface tension as an early response to neural induction (Spemann, 1938).

In the present study, new surface tension values were determined for two sets of deep ectoderm samples (Fig. 1). These were deep dorsal ectoderm immediately posterior to the blastocoel roof, which had briefly been underlain by the advancing roof of the archenteron, and deep ectoderm of the blastocoel roof itself, which had not yet been thus underlain. We report here that the surface tension of the underlain ectoderm (1.60 ± 0.25 dyne/cm) is twice that of the blastocoel roof ectoderm (0.80 ± 0.07 dyne/cm) immediately anterior to it. This helps to explain the wide range of the deep ectoderm surface tension values initially reported. (The higher mean value of the earlier determination (Davis, 1984) may reflect the use of some dorsal ectoderm samples which had been underlain and/or cultured for longer times than those reported here in Table 2.)

Tissue Surface Tensions and Neural Plate Envelopment

The greater surface tension of the underlain portion of the dorsal ectoderm correlates with the onset of the latter tissue's induction to form the neural plate. Chick N-cadherin (Hatta and Takeichi, 1986) and *Xenopus* N-CAM mRNA (Kintner and Melton, 1987) arise at about this time in the neural plate, a tissue which, in explants of amphibian tissues, becomes enveloped not only by uncoated endoderm and mesoderm but also by uncoated epidermis (Townes and Holtfreter, 1955). It has been shown that increased expression of adhesion molecules by cell aggregates in culture results in their envelopment by otherwise identical cell aggregates which have not experienced such an increase (Steinberg and Takeichi, 1994) and also that such increased expression of adhesion molecules correspondingly elevates aggregates' surface tensions (Foty and Steinberg, 1995b).

We propose that this increased surface tension of the prospective neural plate reflects changes in the adhesive prop-

[4] The numbers of mesoderm and endoderm aggregates reported in Davis (1984) Table 1 were inadvertently transposed. There were, in fact, nine mesoderm aggregates and six endoderm aggregates.

erties of its cells which, in turn, have two major morphogenetic consequences. First, cells induced to become neural or sensory may be prevented from mingling with cells fated to become epidermis, i.e., these cell populations become mutually immiscible. Second, by increasing the surface tension of the developing neural plate, these changes in cell adhesion may alter the balance of local forces, causing neural tissue to be enveloped by contiguous mesoderm and ectoderm. Such an increase in cohesiveness could itself be due to the summated effects of the appearance of adhesion molecules such as N-cadherin and N-CAM, partially offset by the disappearance of E-cadherin (L-CAM) in their surfaces (Thiery *et al.*, 1984) at about the same time.

Further contributing to the change in the local balance of forces at the time of neural folding must be the secretion of basal lamina constituents at the boundary between neural plate and epidermis following the beginnings of their epithelialization, documented for both mouse and chick embryos (Martins-Green, 1988). These developments must contribute to changes in the adhesiveness and thus the surface tension at the boundary between neural plate and epidermis. The adhesive relationships involving the developing neural plate and its neighboring tissues would generate a new set of tissue surface tensions, which would in turn specify a new equilibrium configuration in which the latter tissues envelop the neural primordium. Such a mechanism is consistent with the earlier observation that chick embryonic ''neural fold elevation, rather than being driven by neuroepithelial cell wedging, is driven, at least in part, by extrinsic forces generated by lateral nonneuroepithelial tissues'' (Smith and Schoenwolf, 1991; see also Schoenwolf, 1988).

A previous attempt to measure the relative ''adhesiveness'' of ectodermal, mesodermal, and neural cells led to the conclusion that chick embryonic neural tube cells are less adhesive to one another than are cells of the lateral ectoderm to one another (Bellairs *et al.*, 1978). However, what was measured in that case was not the adhesive free energy (a thermodynamic parameter; Phillips, 1969) but the rate of initiation of adhesions between dissociated cells, a kinetic parameter that bears no fixed relationship to the strengths of fully established adhesions or to the tissue surface tensions which they engender (Moyer and Steinberg, 1976; Steinberg, 1996).

The fact that neural epithelial structures will reconstruct themselves internally to an outer covering of epidermis even after the random intermixing of their component cells (Townes and Holtfreter, 1955) clearly shows that these strata are not produced by the execution of a fixed sequence of ''marching orders.'' The precise morphogenetic movements by which this organization is normally achieved must therefore represent, not prechoreographed events, but the immediate responses of the mobile tissues to the force vectors generated by their adhesive interactions. It is significant that the mechanism proposed here for positioning the neural primordium specifies the final arrangement of tissues rather than any particular pathway by which the neural plate sinks below the body surface, for among the chordates a surprising variety of pathways are utilized to achieve this result. These include (i) the folding of the neural plate into a tube and subsequent delamination (as in the anterior regions of neurulae of most higher vertebrates); (ii) its precocious delamination from the epidermis and envelopment, while still open, by epidermal spreading (as in Amphioxus: Hatschek, 1881; Conklin, 1932); and (iii) its submergence as a solid ''neural keel'' which later cavitates (as in teleost, ganoid, and cyclostomatous fishes: Dean, 1896; Wilson, 1899; deSelys-Longchamps, 1910). Even in a given individual, in the absence of genetic differences, anterior and posterior portions of the neural tube may form via different morphogenetic pathways (e.g., Schoenwolf, 1991). Tensions generated by ''cell wedging'' cannot be solely responsible for the final arrangement (Schoenwolf, 1988). All of the above modalities of neural tube positioning are readily accounted for as cell rearrangements promoted by adhesive changes within and between differentially adhesive cell populations, leading toward an anatomical organization in which interfacial (adhesive) free energy is minimized. Thus the striking differences among the various procedures used by chordate embryos to form a neural tube may be understood less as fundamental evolutionary divergences in the underlying mechanisms than as the physical consequences arising from ''heterochrony'': differences in the timing of such events as the appearance or disappearance of nonadhesive neuroepithelial apical domains and the appearance or loss of particular adhesion molecules.

Many details of the morphology both of the developing neural tube and of its component cells (Schroeder, 1970; Jacobson, 1981, 1985, 1991; Jacobson *et al.*, 1986; Smith and Schoenwolf, 1991) remain to be explained, and we do not propose that tissue liquidity persists beyond the time when the tissues' behavior gives evidence of it. Indeed, if increased cell binding, manifested initially as a rising tissue-medium surface tension, eventually became so strong as to inhibit cell slippage, neural ectoderm could then be converted from an increasingly viscous-liquid tissue into a deformable-solid tissue. It seems relevant to note here that the envelopment of one body by another requires liquidity only on the part of the latter, as is the case when a liquid spreads on a solid surface. Thus, submergence of the neural primordium might sometimes take place despite the loss by some or all of its cells of their propensity for liquid-like rearrangement. Our results here, however, demonstrate that tissue cohesiveness begins to increase without any loss of tissue liquidity during the earliest stages of *R. pipiens* neural induction.

Tissue Liquidity and Morphogenetic Mechanisms

Epithelial sheets with component cells firmly linked to one another resemble flexible solids. Thickening, thinning, and bending deformations of such sheets could be generated by active changes in cell shape produced by intracellular structures. Tissue liquidity in underlying cell layers would

facilitate such epithelial contouring by permitting passive, deep tissue compliance to the molding movements of solidlike surface layers. On the other hand, deep, multilayered tissues can migrate actively, *en masse*, with only transient cell distortions, as in the movement of deep mesoderm around the blastopore lip and then in-between ectoderm and endoderm. These thick-tissue migrations are difficult to explain by solid tissue deformation but are readily explained by liquid tissue flow (Phillips, 1984). In such cases, cohering cells must be capable of sliding past one another, just as molecules in ordinary liquids slip past one another to dissipate internal shear stresses.

We have shown here that deep mesoderm and deep ectoderm possess the fundamental property of tissue liquidity (Phillips, 1969; Steinberg and Poole, 1982), characterized by area-invariant tissue surface tensions. Tissue liquidity, arising from the mobility of mutually adhesive cells, has previously been established for deep endoderm by observations that initially stretched cells within continuously compressed endoderm aggregates rapidly (within 15 min) return to their original, undistorted shapes (Phillips and Davis, 1978). Thus both physical measurements and interior cell movements demonstrate that these cell populations respond to applied forces of deformation in the manner of elasticoviscous liquids rather than in the manner of elastic solid bodies (Phillips, 1969, 1984; Phillips and Steinberg, 1978; Phillips *et al.*, 1977a).

The aggregate–medium surface tension measurements presented here and earlier (Davis, 1984) verify the existence of significant, tissue-specific differences in the cohesiveness of the deep germ layers of *R. pipiens* gastrulae. These measurements confirm what Holtfreter asserted (quoted at the outset) but could not verify and what the DAH has predicted on the basis of behavioral evidence: that subsurface ectoderm is more cohesive than subsurface mesoderm, which is more cohesive than subsurface endoderm. In addition, we have found in deep, dorsal ectoderm, shortly after it is underlain by the advancing roof of the archenteron, a significant increase in cohesiveness that precedes and we propose contributes to the subsequent envelopment of neural by epidermal ectoderm and the mutual segregation of these two tissues.

A complete physical explanation of the mutual ''affinities'' of these tissues would require, in addition to the tissue–medium surface tensions measured here, measurement of the interfacial (tissue–tissue) tensions at their boundaries with each other. As a reflection of the adhesiveness of one tissue to another, such interfacial tensions specify miscibility and immiscibility and, in the case of immiscibility, influence the extent to which one liquid body will spread over another (Steinberg, 1964, 1970; Phillips, 1969). For example, it has been shown that the migration of amphibian gastrular mesoderm cells on the wall of the blastocoel is mediated by cell surface $\alpha 5\beta 1$ integrin receptors and extracellular fibronectin fibrils (reviewed by Boucaut *et al.*, 1991). By increasing the adhesion between these two tissues, this interaction would lower the interfacial tension and therefore the resistance to expansion of the mesoderm–ectoderm interface.

Methods for measuring such tissue interfacial tensions have yet to be developed. The tensions at ordinary liquid–liquid or liquid–solid interfaces are normally measured by the determination of contact angles at or near shape equilibrium, but such angles exist only when spreading is incomplete due to relatively low adhesion across the interface. The great majority of embryonic tissue pairs examined show complete spreading of the less cohesive tissue over the more cohesive one (Steinberg, 1970; Foty *et al.*, 1996) and therefore are unsuitable to this approach. ''Distractive'' or kinetic methods of measuring ''cell–cell adhesiveness,'' involving the separation of cells by the application of measured forces or measurement of rates of initiation of adhesions between cells, do not measure the required thermodynamic parameter (reviewed in Steinberg, 1964, pp. 359–361, 1996). Although such interfacial tension values remain to be measured, our tissue–medium surface tension measurements (taken together with the known role of ''coated'' tissues in reversing the inside-out positioning that subsurface germ layers adopt in their absence) fall in the precise sequence required to explain the stratification of these germ layers in the frog gastrula and the ensuing submergence of the neural primordium in the neurula. These findings confirm that Holtfreter's ''tissue affinities'' are physically expressed as tissue surface tensions: well-defined morphogenetic forces arising from intercellular adhesions.

ACKNOWLEDGMENTS

We are grateful to Sandra Mitchell and Peggy MacQueen for their expert technical assistance in this work and to Kara Freshour and Jennie Halpern for the illustrations in Fig. 1. This research was supported by NSF Grants GB-40041 and PCM 78-05903 to H.M.P., by NIH Grant HD30345 to M.S.S., and by a grant to M.S.S. from the Fisher Memorial Trust. G.S.D. was supported by a Summer Research Fellowship from Valparaiso University and by a grant from the Gunther Memorial.

REFERENCES

Adamson, A. W. (1967). ''Physical Chemistry of Surfaces.'' Wiley, New York.

Armstrong, P. B. (1989). Cell sorting out: The self-assembly of tissues in vitro. *Crit. Rev. Biochem. and Mol. Biol.* **24,** 119–149.

Bellairs, R., Curtis, A. S. G., and Sanders, E. J. (1978). Cell adhesiveness and embryonic differentiation. *J. Embryol. Exp. Morphol.* **46,** 207–213.

Boucaut, J.-C., Darribere, T., Shi, D. L., Riou, J.-F., Johnson, K. E., and Delarue, M. (1991). *In* ''Gastrulation: Movements, Patterns and Molecules'' (R. Keller, W. H. Clark, Jr., and F. Griffin, Eds.), pp. 169–184. Plenum, New York.

Cole, K. S. (1932). Surface forces of the *Arbacia* egg. *J. Cell. Comp. Physiol.* **1,** 1–9.

Conklin, E. G. (1932). The embryology of *Amphioxus. J. Morphol.* **54,** 69–151.

Davis, G. S. (1984). Migration-directing liquid properties of embryonic amphibian tissues. *Am. Zool.,* **24,** 649–655.

Dean, B. (1896). The early development of *Amia. Q. J. Microsc. Sci. (New Series)* **38,** 413–444.

deSelys-Longchamps, M. (1910). Gastrulation et formation des feuillets chez *Petromyzon planeri. Arch. Biol., Paris.* **25,** 1–75.

Foty, R. A., Forgacs, G., Pfleger, C. M., and Steinberg, M. S. (1994). Liquid properties of embryonic tissues: Measurement of interfacial tensions. *Phys. Rev. Lett.* **72,** 2298–2301.

Foty, R. A., Pfleger, C. M., Forgacs, G., and Steinberg, M. S. (1996). Surface tensions of embryonic tissues predict their mutual envelopment behavior. *Development* **122,** 1611–1620.

Foty, R. A., and Steinberg, M. S. (1995a). Liquid properties of living cell aggregates: Measurement and morphogenetic significance of interfacial tensions. *In* ''Interplay of Genetic and Physical Processes in the Development of Biological Form'' (D. Beysens, G. Forgacs, and F. Gaill, Eds.), pp. 62–73. World Scientific Co., Singapore.

Foty, R. A., and Steinberg, M. S. (1995b). Differential adhesion specifies envelopment behavior of embryonic and genetically engineered tissues in vitro. *Mol. Biol. Cell* **6,** 207a.

Glazier, J. A., and Graner, F. (1993). Simulation of the differential adhesion-driven rearrangement of biological cells. *Phys. Rev. E* **47,** 2128–2154.

Glazier, J. A., Raphael, R. C., Graner, F., and Sawada, Y. (1995). The energetics of cell sorting in three dimensions. *In* ''Interplay of Genetic and Physical Processes in the Development of Biological Form'' (D. Beysens, G. Forgacs, and F. Gaill, Eds.), pp. 54–61. World Scientific Co., Singapore.

Hamburger, V. (1960). ''A Manual of Experimental Embryology'' Univ. of Chicago Press, Chicago.

Hatschek, B. (1881). Studien über Entwicklung des *Amphioxus. Arb. Zool. Inst. Wien,* **4,** 1–88.

Hatta, K., and Takeichi, M. (1986). Expression of N-cadherin adhesion molecules associated with early morphogenetic events in chick development. *Nature* **320,** 447–449.

Heintzelman, K. F., Phillips, H. M., and Davis, G. S. (1978). Liquid-tissue behavior and differential cohesiveness during chick limb budding. *J. Embryol. Exp. Morphol.* **47,** 1–15.

Hodgman, C. D. (1958). ''Handbook of Chemistry and Physics'' Chemical Rubber Publishing Co., Cleveland.

Holtfreter, J. (1939). Gewebeaffinität, ein Mittel der embryonalen Formbildung. *Arch. Exp. Zellforsch. Besonders Gewebezücht.* **23,** 169–209; (Revised and reprinted in English, 1964). *In* ''Foundations of Experimental Embryology'' (B. H. Willier and J. M. Oppenheimer, Eds.), pp. 186–225. Prentice–Hall, Englewood Cliffs, NJ.

Holtfreter, J. (1943). Properties and functions of the surface coat in amphibian embryos. *J. Exp. Zool.* **93,** 251–323.

Holtfreter, J. (1944). A study of the mechanics of gastrulation, II. *J. Exp. Zool.* **95,** 171–212.

Jacobson, A. G. (1967). Amphibian cell culture, organ culture, and tissue dissociation. *In* ''Methods in Developmental Biology'' (N. Wessels and R. Wilt, Eds.), pp. 531–542. Crowell, New York.

Jacobson, A. G. (1981). Morphogenesis of the neural plate and tube. *In* ''Morphogenesis and Pattern Formation'' (T. G. Connelly, Ed.), pp. 233–263. Raven Press, New York.

Jacobson, A. G. (1985). Adhesion and movement of cells may be coupled to produce neurulation. *In* ''The Cell in Contact: Adhesions and Junctions as Morphogenetic Determinants'' (G. M. Edelman and J.-P. Thiery, Eds.), pp. 49–65. Wiley, New York.

Jacobson, A. G. (1991). Experimental analyses of the shaping of the neural plate and tube. *Am. Zool.,* **31,** 628–643.

Jacobson, A. G., Oster, G. F., Odell, G. M., and Cheng, L. Y. (1986). Neurulation and the cortical tractor model for epithelial folding. *J. Embryol. Exp. Morphol.* **96,** 19–49.

Kintner, C. R., and Melton, D. A. (1987). Expression of *Xenopus* N-CAM RNA in ectoderm is an early response to neural induction. *Development,* **99,** 311–325.

Martins-Green, M. (1988). Origin of the dorsal surface of the neural tube by progressive delamination of epidermal ectoderm and neuroepithelium: Implications for neurulation and neural tube defects. *Development* **103,** 687–706.

Mombach, J. C. M., Glazier, J. A., Raphael, R. C., and Zajac, M. (1995). Quantitative comparison between differential adhesion models and cell sorting in the presence and absence of fluctuations. *Phys. Rev. Lett.* **75,** 2244–2247.

Moyer, W. A., and Steinberg, M. S. (1976). Do rates of intercellular adhesion measure the cell affinities reflected in cell-sorting and tissue spreading configurations? *Dev. Biol.* **52,** 246–262.

Phillips, H. M. (1969). ''Equilibrium Measurements of Embryonic Cell Adhesiveness: Physical Formulation and Testing of the Differential Adhesion Hypothesis.'' Ph.D. dissertation, Johns Hopkins University, Baltimore, MD.

Phillips, H. M. (1984). Physical analysis of tissue mechanics in amphibian gastrulation: *Am. Zool.* **24,** 657–672.

Phillips, H. M., and Davis, G. S. (1978). Liquid–tissue mechanics in amphibian gastrulation: Germ-layer assembly in *Rana pipiens. Am. Zool.* **18,** 81–93.

Phillips, H. M., and Steinberg, M. S. (1969). Equilibrium measurements of embryonic chick cell adhesiveness. I. Shape equilibrium in centrifugal fields. *Proc. Natl. Acad. Sci. USA* **64,** 121–127.

Phillips, H. M., and Steinberg, M. S. (1978). Embryonic tissues as elasticoviscous liquids. I. Rapid and slow shape changes in centrifuged cell aggregates. *J. Cell Sci.* **30,** 1–20.

Phillips, H. M., Steinberg, M. S., and Lipton, B. (1977a). Embryonic tissues as elasticoviscous liquids. II. Direct morphological evidence for cell slippage in centrifuged aggregates. *Dev. Biol.* **59,** 124–134.

Phillips, H. M., Wiseman, L. L., and Steinberg, M. S. (1977b). Self vs nonself in tissue assembly: Correlated changes in recognition behavior and tissue cohesiveness. *Dev. Biol.* **57,** 150–159.

Poole, T. J., and Steinberg, M. S. (1977). SEM-aided analysis of morphogenetic movements: Development of the amphibian pronephric duct. *IIT Res. Inst. Semin. 1977* **II,** 43–52.

Rowlinson, J. S., and Widom, B. (1989). ''Molecular Theory of Capillarity.'' Clarendon Press, Oxford.

Rugh, R. (1962). ''Experimental Embryology Techniques and Procedures.'' Burgess, Minneapolis.

Schoenwolf, G. C. (1988). Microsurgical analyses of avian neurulation: Separation of medial and lateral tissues. *J. Comp. Neurol.,* **276,** 498–507.

Schoenwolf, G. C. (1991). Cell movements in the epiblast during gastrulation and neurulation in avian embryos. *In* ''Gastrulation: Movements, Patterns and Molecules'' (R. Keller, W. H. Clark, Jr., and F. Griffin, Eds.), pp. 1–28. Plenum, NY.

Schroeder, T. E. (1970). Neurulation in *Xenopus laevis.* An analysis and model based upon light and electron microscopy. *J. Embryol. Exp. Morphol.* **23,** 427–462.

Shumway, W. (1940). Stages in the normal development of *Rana pipiens.* I. External form. *Anat. Rec.* **78,** 139–148.

Smith, J. L., and Schoenwolf, G. C. (1991). Further evidence of extrinsic forces in bending of the neural plate. *J. Comp. Neurol.* **307,** 225–236.

Spemann, H. (1938). ''Embryonic Development and Induction.'' Yale Univ. Press, New Haven, CT.

Steinberg, M. S. (1962a). On the mechanism of tissue reconstruction by dissociated cells. I. Population kinetics, differential adhesiveness, and the absence of directed migration. *Proc. Natl. Acad. Sci. USA* **48,** 1577–1582.

Steinberg, M. S. (1962b). Mechanism of tissue reconstruction by dissociated cells. II. Time-course of events. *Science* **137,** 762–763.

Steinberg, M. S. (1962c). On the mechanism of tissue reconstruction by dissociated cells. III. Free energy relations and the reorganization of fused, heteronomic tissue fragments. *Proc. Natl. Acad. Sci. USA* **48,** 1769–1776.

Steinberg, M. S. (1963). Tissue reconstruction by dissociated cells. *Science* **141,** 401–408.

Steinberg, M. S. (1964). The problem of adhesive selectivity in cellular interactions. *In* ''Cellular Membranes in Development'' (M. Locke, Ed.), pp. 321–366. Academic Press, New York.

Steinberg, M. S. (1970). Does differential adhesion govern self-assembly processes in histogenesis? Equilibrium configurations and the emergence of a hierarchy among populations of embryonic cells. *J. Exp. Zool.* **173,** 395–433.

Steinberg, M. S. (1996). Adhesion in development: An historical overview. *Dev. Biol.* **180,** 377–388.

Steinberg, M. S., and Poole, T. J. (1982). Liquid behavior of embryonic tissues. *In* ''Cell Behaviour'' (R. Bellairs, A. S. G. Curtis, and G. Dunn, Eds.), pp. 583–607. Cambridge Univ. Press, Cambridge, England.

Steinberg, M. S., and Takeichi, M. (1994). Experimental specification of cell sorting, tissue spreading and specific spatial patterning by quantitative differences in cadherin expression. *Proc. Natl. Acad. Sci. USA* **91,** 206–209.

Thiery, J.-P., Delouvee, A., Gallin, W. J., Cunningham, B. A., and Edelman, G. M. (1984). Ontogenetic expression of cell adhesion molecules: L-CAM is found in epithelia derived from the three primary germ layers. *Dev. Biol.* **102,** 61–78.

Townes, P. L., and Holtfreter, J. (1955). Directed movements and selective adhesion of embryonic amphibian cells. *J. Exp. Zool.* **128,** 53–120.

Trinkaus, J. P., and Lentz, J. P. (1964). Direct observation of type-specific segregation in mixed cell aggregates. *Dev. Biol.* **9,** 115–136.

Vogt, W. (1929). Gestaltungsanalyse am Amphibienkeim mit ortlicher Vitalfarbung. II. Teil. Gastrulation and Mesodermbildung bei Urodelen und Anuren. *Arch. EntwMech. Org.* **120,** 384–706.

Wilson, H. V. (1899). The embryology of the sea bass (*Serranus atrarius*). *Bull. U.S. Fish Comm.* **9,** 209–277.

Wiseman, L. L., Steinberg, M. S., and Phillips, H. M. (1972). Experimental modulation of intercellular cohesiveness: Reversal of tissue assembly patterns. *Dev. Biol.* **28,** 498–517.

Yoneda, M. (1964). Tension at the surface of sea-urchin egg: A critical examination of Cole's experiment. *J. Exp. Biol.* **41,** 893–906.

Received for publication February 26, 1997
Accepted September 10, 1997